UNIVERSITY OF CALIFORNIA
RIVERSIDE

Vanadium Oxidation and Retention by Iron and Manganese Oxides

A Thesis submitted in partial satisfaction
of the requirements for the degree of

Master of Science

in

Environmental Science

by

Amy Kirsten Salvador

September 2017

Thesis Committee:

- Dr. Samantha C. Ying, Chairperson
- Dr. Haizhou Liu
- Dr. Robert C. Graham
- Dr. Suveen Mathaudhu

The Thesis of Amy Kirsten Salvador is approved:

_____

_____

_____

_____

Committee Chairperson

University of California, Riverside

ABSTRACT OF THE THESIS

Vanadium Oxidation and Retention by Iron and Manganese Oxides

by

Amy Kirsten Salvador

Master of Science, Graduate Program in Environmental Sciences
University of California, Riverside, September 2017
Dr. Samantha Ying, Chairperson

Vanadium (V) is a ubiquitous redox active transition metal found in soil systems, which can have adverse effects on the neurological development of children when ingested. Human exposure to vanadium can occur via consumption of contaminated groundwater containing V that is mobilized from soils and sediments under redox-fluctuating conditions. V is predominantly present in the more mobile V(V) form under oxidizing conditions; however, specific biological and geochemical processes contributing to vanadium redox cycling and subsequent change in its mobility into groundwater systems is not well understood. Past studies have demonstrated that permanganate is a strong oxidant of V, rapidly oxidizing V(IV) to V(V) upon contact. Therefore, we hypothesize that naturally-occurring manganese (Mn) oxides, such as birnessite, could be a potential oxidant of V in soils and sediment systems. Furthermore, iron (Fe) and manganese oxides are important components of soil systems as possible sorbents of vanadium. To understand the fate

and transport of V, a Donnan reactor that simulates diffusion-limited environments within soils was used to examine V(IV) oxidation and subsequent sorption of V(V) on Mn and Fe oxides. V sorption and oxidation was monitored over time by measuring the concentration of aqueous V using ICP-OES in conjunction with Fe speciation determined by ferrozine assay. X-ray absorption spectroscopy (EXAFS and XANES analysis) and SEM-EDX imaging was used to determine changes in Mn oxide structure and speciation of adsorbed V over time. The oxidation of V resulting from contact with birnessite, with subsequent reductive dissolution of the oxidant, will affirm the potential role of V transformation from V(IV) to V(V) by Mn oxides. The results of this study demonstrate that the presence of naturally-occurring Fe and Mn oxides in soils and sediments can impact the fate and transport of V in natural systems and their role in controlling V mobilization into water resources.

TABLE OF CONENTS

Abstract iv
Table of Contents vi
List of Figures vii
1 Introduction 1
2 Materials and Methods 4
2.1 Birnessite synthesis and goethite characterization 4
2.2 Donnan experiment conditions 5
2.3 Aqueous phase analysis 7
2.4 Ferrozine assay of 90 mM V(IV) and goethite incubations 8
2.5 Solid phase analysis 8
3 Results 9
3.1 Aqueous dynamics within the Donnan reactor 9
3.1.1 Oxidation and retention of V by birnessite 9
3.1.2 Competitive oxidation and retention of V by goethite and birnessite 12
3.1.3 Oxidation of V(IV) by Fe oxides 16
3.2 Solid phase acid digestion analysis 17
3.3 EXAFS and XANES analysis of adsorbed V 19
3.4 Scanning electron microscopy and EDX analysis on solid phase 23
3.5 X-ray diffraction analysis of solid phase 27
4 Discussion 29
5 Conclusion 32
References 34
Supplemental Information 37

List of Figures

Figure 1 Schematic of Donnan reactor 6,7
Figure 2 Colors of V(IV) and V(V) oxidation states.....10
Figure 3 Aqueous concentrations of 90 mM V(IV) and birnessite.....11
Figure 4 Aqueous concentrations of 20 μM V(IV) with birnessite and goethite.....13
Figure 5 Aqueous concentrations of 200 μM V(IV) with birnessite and goethite.....15
Figure 6 Ferrozine assay of 90 mM V(IV) and goethite incubation.....16
Figure 7 Solid phase concentrations of 20 μM V(IV) experiment.....18
Figure 8 Solid phase concentrations of 200 μM V(IV) experiment.....19
Figure 9 Fractional distribution of V(IV) to V(V) in 90 mM experiment.....21
Figure 10 Fractional distribution of V(IV) to V(V) in 20 and 200 μM experiments 22
Figure 11 SEM images of birnessite and goethite chambers 24
Figure 12 SEM-EDX image and spectra of birnessite chamber at 96 hours.....26
Figure 13 XRD patterns of birnessite and goethite chambers 28

Introduction

Vanadium (V) is a naturally-occurring trace metal found in many oxidation states with V(IV) and V(V) as the most ubiquitous in aquifer sediment systems (Hem, 1985). V is found in mafic igneous and sedimentary minerals as V^{3+} which can readily substitute for Fe^{3+} and Al^{3+} within the mineral structure (Wright and Belitz, 2010). The second largest reservoir of V in earth's surface environments aside from ocean sediment reside in soil with 3.4×10^{10} tons and 2.7×10^{9} tons of V cycled in surface water (Hope, 2008). Surface and groundwater rarely exceeds V concentrations of 10 µg L^{-1}, though areas of US have exhibited higher concentrations up to 50 µg L^{-1} in groundwater and surface water via steel and uranium mining and metallurgy, the burning and mining of fossil fuels, and wastewater from electronic industries (USGS).

Vanadium in natural drinking water sources, is considered hazardous to human health in concentrations exceeding 50 µg L^{-1} as determined by the California Department of Health. Prolonged exposure to V(V), the most toxic form of V, via inhalation results in respiratory irritation and bronchitis, while exposure through ingestion through drinking-water increases risks in neurological impairment and cancer (World Health Organization, 1988; Olopade and Connor, 2011).

Concentrations of V(V) in groundwater is dependent upon dissolved oxygen concentration and presence of oxides such as Mn and Fe oxides. V is very reactive under various redox conditions and V oxidation state is dependent upon Eh and pH (Hem, 1985). Under aerobic and alkaline conditions, vanadium is oxidized to V(V), the generally more mobile oxidation state within groundwater systems. The dominant species of V(V) in soil and

groundwater sediment are oxyanions $H_2VO_4^-$ and HVO_4^{2-}, whereas V(IV) is commonly found as VO^{2+} and $V(OH)_3^+$ oxycations which can form strong inner-sphere complexes with metal oxides and can therefore be immobilized by adsorption (Wehrli and Stumm, 1989).

Redox active soil minerals like Mn and Fe oxides are important to the mobilization and porewater concentration of V. Contact of V(IV) with strong oxidizers such as permanganate ($KMnO_4$) have been found to result in oxidation of V(IV) and increase the release of mobile V(V) (Moore and Hicks, 1975). Mn oxides have a low zero-point charge, high surface area, and high surface charge which attributes to greater specific adsorption potential of cations and a subsequent release of protons (Dixon and White, 2002). Few studies have investigated the interaction of V with Mn(III/IV) oxides, which are abundant in natural soil and sediment systems. Although the rate of oxidation of V(IV) is increased by the presence of hydrous oxides, titanium and aluminum oxides have also been shown to overcome electrostatic repulsion from positively charged vanadate surfaces and form inner-sphere complexes with V(V) (Wehrli and Stumm, 1988). Kinetic results of V(V) with Fe oxides have demonstrated surface sorption in oxic conditions via inner-sphere complexes (Peacock et al., 2004), though V(IV/V) and Fe oxides have not been observed in anoxic environments.

Acidifying and reducing aquatic systems can reduce V from V(V) to V(IV/III) where V(III) is most thermodynamically stable at extremely low Eh and pH conditions (Wright and Belitz, 2010). Biological agents such as dissimilatory metal reducing bacteria (*Shewanella oneidensis* and *Thiobacillus thiooxidans*) have also been shown to reduce V from V(V) to V(IV) in anaerobic conditions (Myers et al., 2004; Briand et al., 1996). In oxygen poor

environments, manganese, iron, and sulfur oxides that coat the exterior of aggregates, can be utilized by *Shewanella* and *Thiobacillus* as electron donors in the reduction of V (Ying et al., 2011; Briand, 1996).

Physical environmental changes such as fluctuations in water table levels impart changes in oxygen availability. The USGS estimated California as the state with the highest groundwater use and that the majority of that water went to irrigation. Increased groundwater pumping for irrigation in the lowlands has changed aquifer environments and increased mixing of aquifer aqueous material. Of these high concentration wells, the majority were in oxic conditions. Central Valley groundwater has experienced levels of V near or above the CA-NL threshold of 50 μg L^{-1} as a result of decreased water table levels from increased pumping (Wright et al., 2014). Induced suboxic zones via decreasing water tables levels provide oxygen to once anoxic environments and generate redox transition zones that are important to the transformation of V.

Soil and sediment aggregate systems contain pores of many sizes that exhibit both advective and diffusive transport into the aggregate interior (Sextone et al., 1985). Due to diffusion-limited transport, oxygen availability is stratified within the aggregate, resulting in oxic conditions on the aggregate exterior and anoxic conditions within the interior (Sextone et al., 1985; Tokunaga et al., 2001).

In this study, we examine the fate and transport of vanadium in simulated redox transition zones within groundwater systems. Birnessite and goethite serve as electron acceptors and sorption surfaces in an anoxic environment. Diffusive transport within aggregates are simulated by a semipermeable membrane that separates Donnan reactor cells. By introduction of V(IV) above and below the concentration at which polynuclear species form

(i.e., approximately 100 μM at circumneutral pH) into the Donnan reactor, we examine V redox cycling and sorption dynamics by analyzing the solid phase on x-ray absorption (i.e., EXAFS and XANES), SEM-EDX, XRD, and solid phase acid digestions in conjunction with ICP-OES. Changes in morphology and crystal structure of oxides were examined using SEM and XRD. Aqueous concentrations were analyzed using ICP-OES,

Our findings show that V(IV) interaction with birnessite leads to reductive dissolution of birnessite and production of V(V), which then subsequently adsorbs on birnessite and goethite after redistribution throughout the Donnan chamber. Fe oxides and V(IV) shows a possible oxidation reaction of V(V) but within a few short bursts in the beginning of the experiment. Overall, the retention and oxidation of V in a solution of Mn and Fe oxides is highly dependent on V(IV) concentration, diffusion limitation, and the sorptive capacities of the oxides.

2. Materials and Methods

2.1 Birnessite synthesis and goethite characterization

Birnessite was synthesized by adding 66 mL of trace metal grade HCl to 63 g of KMnO4 potassium permanganate dissolved in 1 L DDI water and stirred for 10 minutes and heated at 90 °C until dissolved (Mckenzie, 1971). The solution was then cooled for 30 minutes and filtered. The collected solids were washed and filtered several times until filtrate was clear. Solids were then air dried and crushed with mortar and pestle.

Goethite (STREM Chemicals, CAS No. 51274-00-1) was washed with DDI water, dialyzed, and crushed with mortar and pestle before use. Goethite and birnessite were characterized via x-ray diffraction (XRD) using Cu Kα radiation and the surface area was

determined by Brunauer-Emmett-Teller (BET) N_2 adsorption to be 10.5113 $m^2\ g^{-1}$ and 47.0842 $m^2\ g^{-1}$, respectively.

Experiments were performed at room temperature (25 ºC) and anoxic atmosphere (95%N_2:5%H_2) within an anoxic glovebag. The donnan reactor (Figure 1) was constructed using HCl washed 3" PVC pipes with a 0.1 µm polycarbonate filter installed between two elbow chambers to simulate diffusive transport. A solution of brilliant blue was added to one side to check for leakage before the run of the experiment and determine diffusion rate. Oxides were added to each chamber using 1:1.35 mass ratio of birnessite to goethite after being sonicated in background solution of 10 mM PIPES (pH 7) and 0.1 M NaCl (total volume of solution within each chamber was 900 mL) and left to equilibrate for 18 or more hours within the anoxic glovebag. Oxide slurry is then stirred with overhead impellers at approximately 400 rpm overnight before adding V(IV). Initiation of the reaction occurred with the addition of vanadyl sulfate at V(IV) concentrations below and above concentration of polynuclear species formation, 20 µM and 200 µM, respectively (Figure 1A). Additionally, a separate high concentration control was performed on each oxide by reacting birnessite and goethite individually with 90 mM V(IV) (Figure 1B).

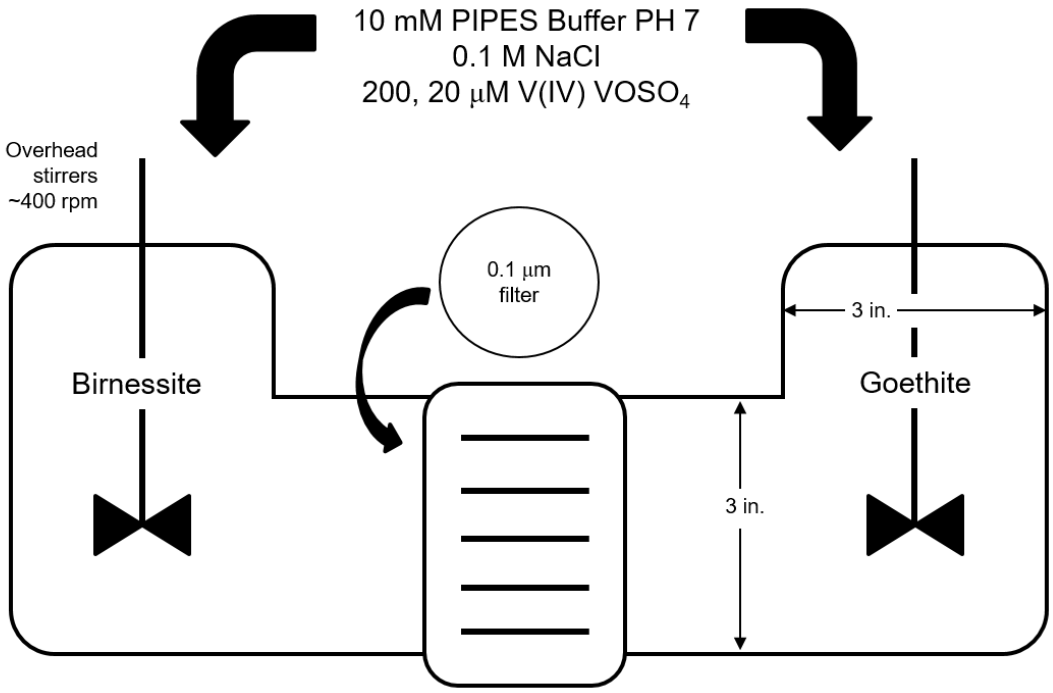

Fig. 1A. Schematic of Donnan reactor simulating diffusive flow of 20 and 200 μM V(IV) experiments with birnessite and goethite.

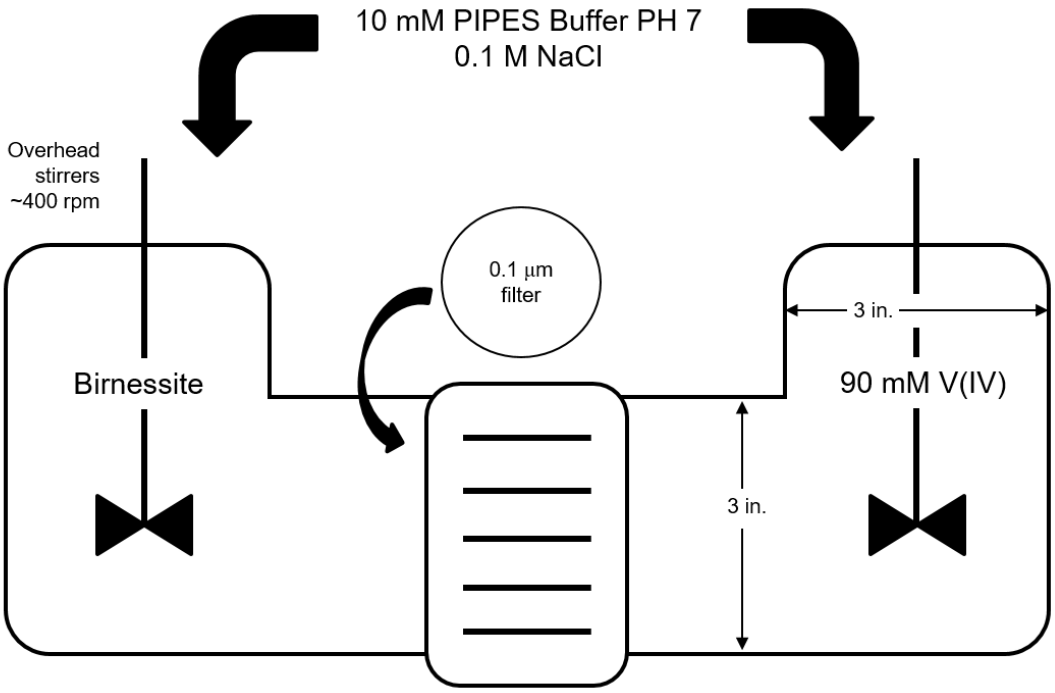

Fig. 1B. Schematic of Donnan reactor simulating diffusive flow of 90 mM V(IV) experiments with birnessite.

2.3 Aqueous phase analysis

Homogenized slurry samples were taken at 30 seconds, 10, 20, 30 minutes, 1, 2, 4, 6, 8, 14, 22, 29, 37, 50, 72, and 96 hours. 3 ml of slurry were passed through 0.2 μm filter and filtrate were collected in 15 ml centrifuge tubes. 3 drops (~20 μl) of concentrated trace metal grade nitric acid were added to aqueous samples and stored at 4 ºC for least 24 hours prior to quantification of aqueous Fe, Mn, and V using ICP-OES to allow PIPES to precipitate from solution. ICP-OES was calibrated (see SI for calibration points and detection limits) with an R^2 value of 1.0 ±0.1.

2.4 Ferrozine assay of 90 mM V(IV) and goethite incubations

90 mM of V(IV) was added to 6.48 g of goethite in 900 mL of 10 mM PIPES (pH 7) and 0.1 M NaCl within the (95%N_2:5%H_2) atmosphere glovebag. 4 mL of slurry were sampled in the same time points as the donnan experiments up to 6 hours. Samples were passed through a 0.2 µm syringe tube. Samples were quickly taken out of the glovebag. 100 µL of 0.01 M ferrozine and 50 µL ammonium acetate buffer adjusted to pH 9.5 with ammonium hydroxide were added to 1 mL of filtered sample and absorbance was read on a spectrophotometer set to 562 nm and calibrated to 90 mM V(IV).

2.5 Solid phase analysis

3 ml of slurry sampled from each Donnan chamber was transferred to preweighed borosilicate tubes for determining total concentration of Mn, Fe, and V within the solid phase. The slurry sample was weighed before and after drying at 90 ºC for 3 days. 2 ml of trace metal grade HCl was then added to the dried sample, mixed thoroughly with a vortex, and placed in a water bath heated to 90 ºC until all solids were dissolved. Sample was diluted with DDI water to 3% acid and kept at 4 ºC for at least 24 hours prior to ICP-OES analysis.

An additional 5 ml of slurry sample from each chamber was taken to determine solid phase V, Mn, and Fe speciation using X-ray absorption spectroscopy at Stanford Synchrotron Radiation Lightsource (Stanford, CA, USA). Solids were collected on ashless filter paper (Whatman) and encased in 0.5 mil or 1 mil Kapton tape and kept anoxic until analysis. Samples were transported in anaerobic boxes and kept anoxic using AnaeroPack-Anaero (Mitsubishi) to SSRL. Samples were then run at beamline 4-3 for V K-edge XANES using

a 100 element Ge detector under liquid nitrogen cryostat. Spectra were analyzed using a titanium filter and collected 230 eV below to 250 eV above the V K-edge of 5465 eV. Ratio of oxidative speciation of V was determined by linear combination fitting against vanadyl sulfate V(IV) and sodium orthovanadate V(V) standards using the Athena program (Ravel and Newville, 2005).

Solid phase was imaged using scanning electron microscopy at UCR Advanced Microscopy Facility. To prepare samples, 5 mL of slurry solution from each chamber was twice washed with acetone and centrifuged at 3300 rpm to remove ions in solution. Centrifuged solid samples were oven dried at 40 ºC prior to SEM and EDX analysis. Stub with samples were then sputter coated with Pd/Au using Cressington sputter coater 108 auto. Samples ran on SEM equipped with energy dispersive detector and analyzed from 1 to 5 µm scale.

Oxide transformation was also assessed using X-ray diffraction analysis from 5-45 °2θ Cu Kα for goethite and birnessite samples. To remove halite peaks at 31.73 °2θ Cu Kα, samples were centrifuged, eluent was decanted, and samples were twice washed with acetone, and oven dried at 40°C before analyzed on XRD.

3. Results

3.1 Aqueous dynamics within the Donnan reactor

3.1.1 Oxidation and retention of V by birnessite

To assess the capacity of birnessite to oxidize and adsorb V(IV), 90 mM V(IV) was injected into the opposing chamber to birnessite within the Donnan reactor (Figure 1A). At high concentration of dissolved V, oxidation state of V can be determined simply by observing the color of the liquid where V(IV) is blue and V(V) is yellow (Figure 2A). Samples taken from birnessite chamber were initially dark brown (Figure 2B) and the presence of V(IV) during injection was confirmed by the blue color of the liquid within the chamber (Figure 2C). The remaining aqueous phase within the birnessite chamber was a yellow-green possibly indicative of the presence of a mixture of V(IV) and V(V) (Figure 2D). By 96 hours, all aqueous phase within the V injection chamber was yellow indicating oxidation of V(IV) to V(V) (Figure 2E) accompanied by complete reductive dissolution of birnessite within the birnessite chamber where no solids were detected at the end of the experimental time. Controls with V(IV) only in centrifuge tubes left within the anoxic glovebag remained blue throughout the experiment. These observations confirm the ability of birnessite to oxidize V(IV) to V(V).

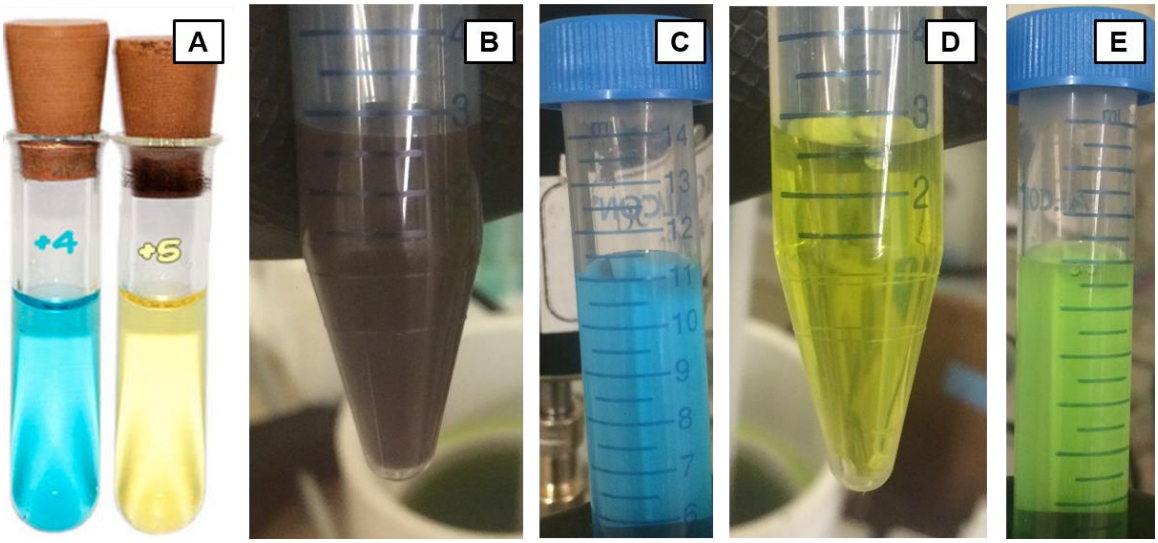

Fig.2. (A) Reference image of colors exhibited by solutions of V(IV) and V(V). (B-E) Unfiltered sample solutions in 90mM total V(IV) concentration experiment. (B) Initial birnessite chamber solution 30 seconds after V(IV) injection. (C) Initial V(IV) injectionchamber solution 30 seconds after V(IV) injection. (D) Final birnessite chamber solution 100 hours after V(IV) injection. (E) Final injection chamber solution 100 hours after V(IV) injection.

Figure 3 shows total aqueous Mn and V concentrations within the aqueous phase of Donnan samples over the course of the experiment. The results show that V diffuses from the injection chamber into the birnessite chamber, reaching approximately 20 mM by 100 hours. Decreased total aqueous concentrations over the experimental time is due to V adsorption on birnessite. Aqueous Mn concentrations increase from 0 to 8 mM within first 24 hours due to reductive dissolution of birnessite mediated by V(IV) oxidation.

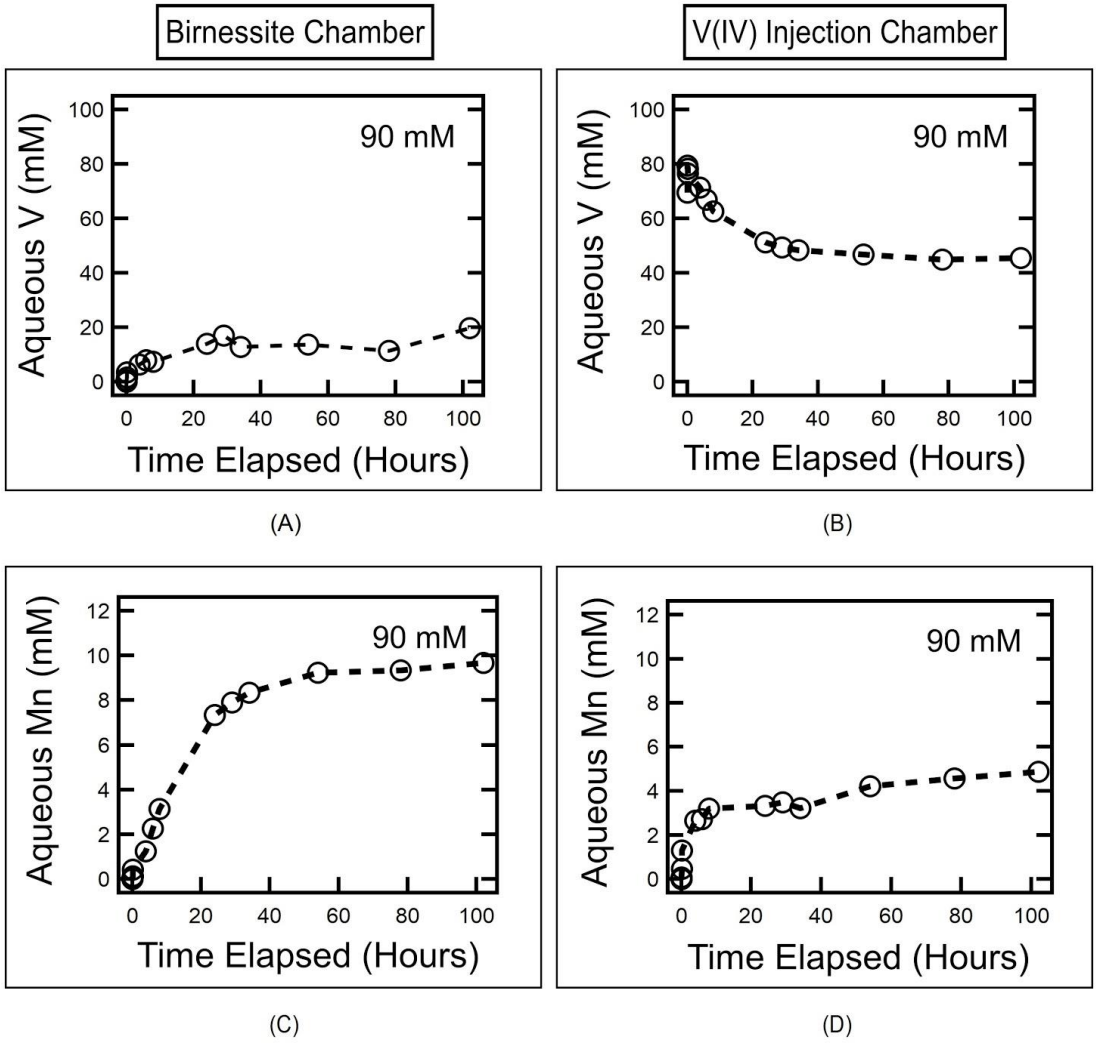

Fig. 3. Aqueous V concentrations in birnessite chamber (A) and V(IV) injection chamber (B), aqueous Mn concentrations in birnessite chamber (C) and V(IV) chamber (D) with initial V(IV) injection concentration of 90 mM with 1.48 g of birnessite oxide in 900 mL 0.1 M NaCl and 10 mM PIPES background.

3.1.2 Competitive oxidation and retention of V by goethite and birnessite

Using the Donnan reactor, we are able to examine the competitive retention of V on birnessite and goethite while also observing redox dynamics. By placing birnessite in one chamber and goethite in the opposing chamber and injecting aqueous V(IV) into both simultaneously (Figure 1A), we can determine the rate of oxidation and retention of V overtime. The competitive experiment was performed at two concentrations of V, one below (20 μM) and above (200 μM) the concentration threshold upon which polynuclear V(V) species are formed (Larson, 1995). Figure 4 shows the total aqueous concentrations of V, Mn, and Fe over the course of the competitive experiment at low V concentration treatment. Total aqueous concentration of V decreases rapidly after injection within both chambers demonstrating sorption onto both oxides (Figure 4A and B). Aqueous concentrations of Mn increase gradually within both chamber upon V oxidation coincident with birnessite reductive dissolution (Figure 4C and D). Aqueous Mn concentrations exceed V injection chamber at the end of the experimental time possibly due to detection of Mn nanoparticles or release of entrained Mn within birnessite solids. Aqueous Fe concentration within the birnessite chamber remained near or below detection limit throughout the experiment (Figure 4E); aqueous Fe concentrations demonstrated occasional low concentration spikes within the goethite chamber within the first 6 hours of the experiment, then decreasing to near detection limit for the remainder of the experiment (Figure 4F).

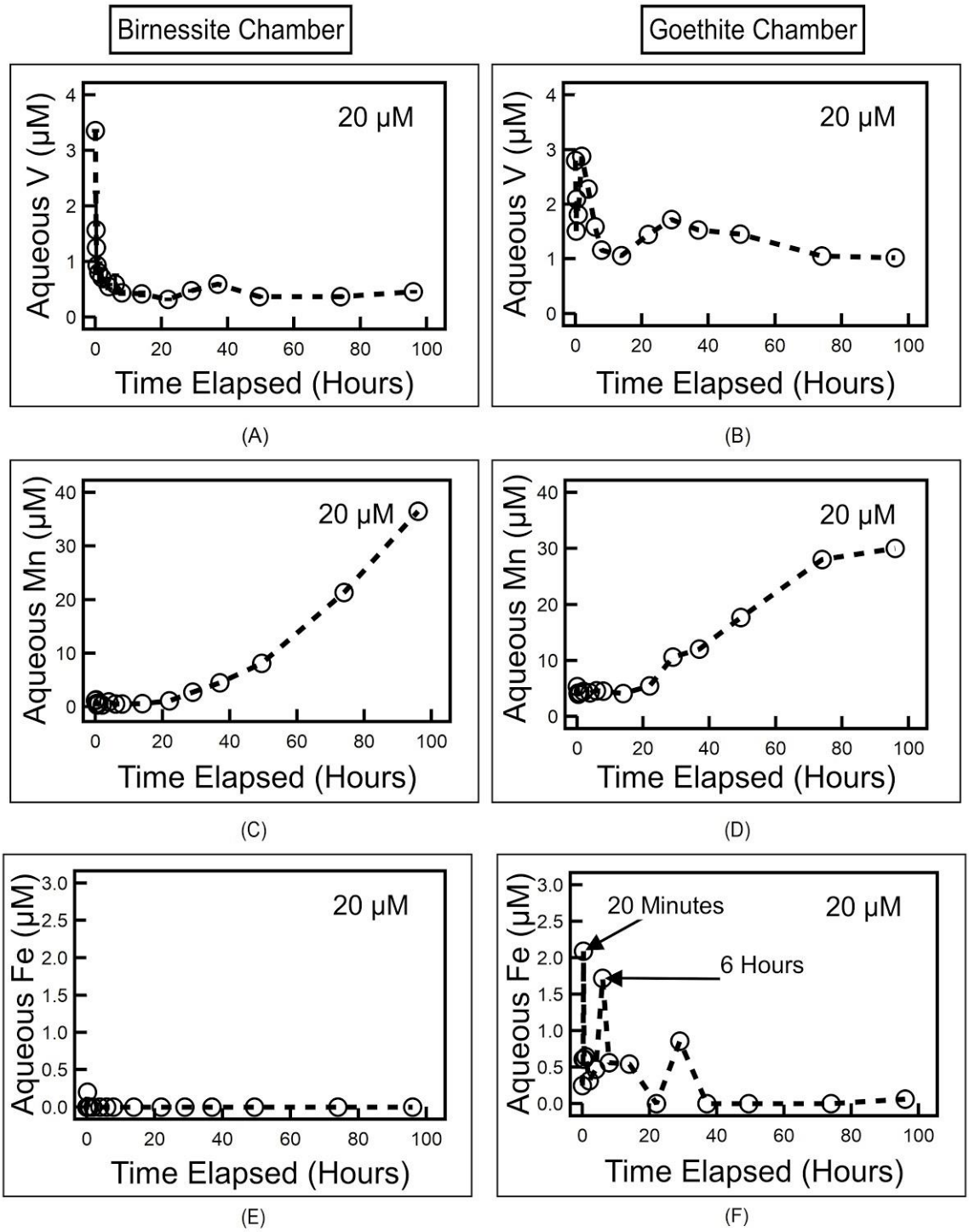

Fig.4. Aqueous V (A,B), Mn (C,D), and Fe (E,F) concentrations from 20 μM V(IV) experiment sampled from birnessite chamber (left panel) and goethite chamber (right panel). Samples filtered (0.2 μm).

During the high V concentration treatment at 200 μM, aqueous V, Mn, and Fe dynamics showed drastically different behavior as compared results from the low concentration treatment (Figure 5). Upon addition of V to both chambers, a similar decrease in total V was observed in the birnessite chamber as the low treatment likely resulting from rapid adsorption (Figure 5A); however, within the goethite chamber, an initial spike in V was not observed and instead a peak was detected at 6 hours after injection (Figure 5B). Aqueous Mn concentrations also did not demonstrate the same behavior as during low treatment; after injection, aqueous Mn concentrations remained low throughout the experimental time, reaching a maximum concentration of 1 and 2 μM within the birnessite and goethite chambers, respectively (Figure 5C and D). Aqueous Fe concentrations also remained at or below detection limit within the birnessite chamber throughout the experiment, similar to low concentration treatment results (Figure 5E), but concentrations of aqueous Fe reached nearly 15 μM within 30 minutes followed by a graduate decrease to near detection limit by 50 hours (Figure 5F).

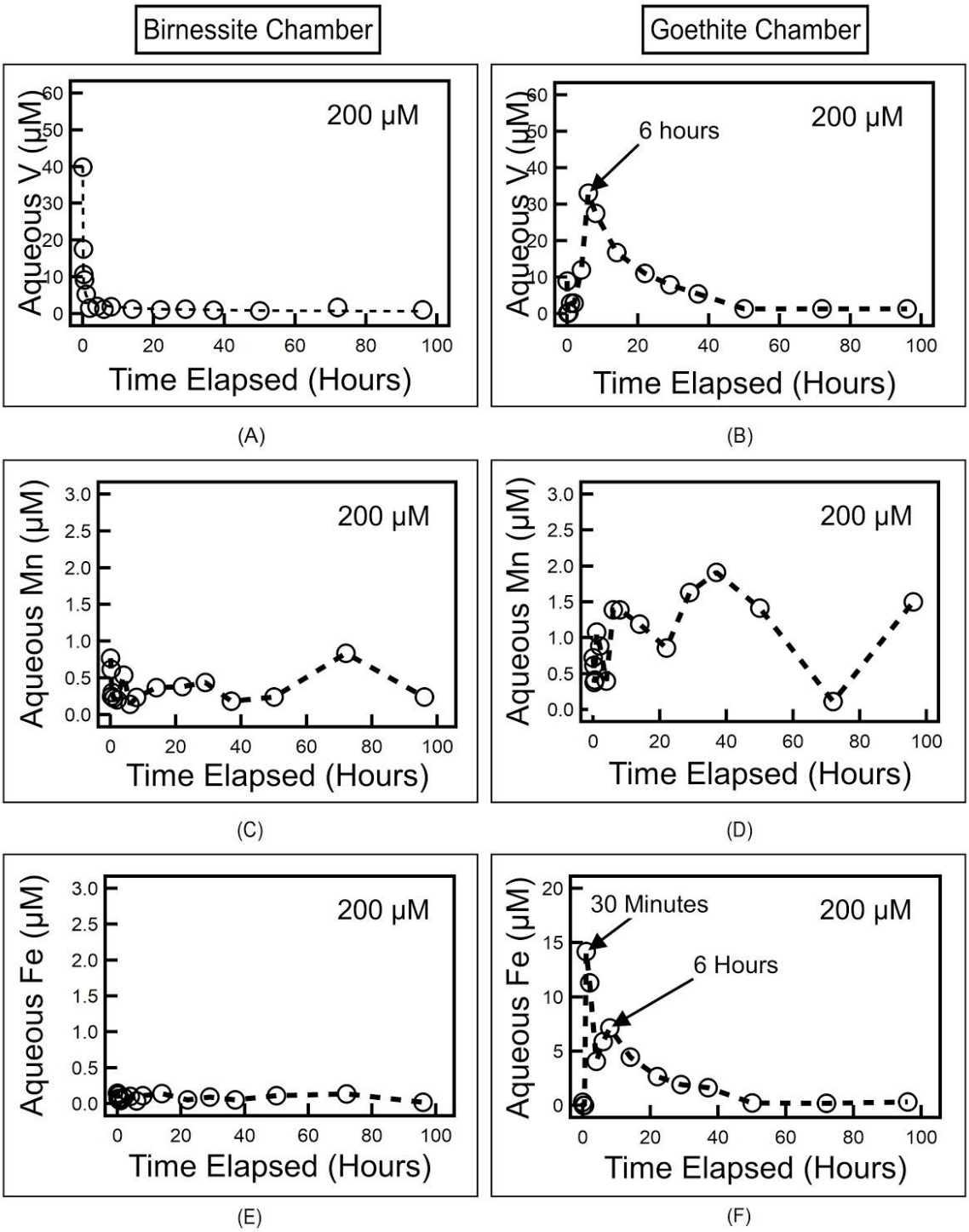

Fig.5. Aqueous V (A,B), Mn (C,D), and Fe (E,F) concentrations from 200 μM V(IV) experiment sampled from birnessite chamber (left panel) and goethite chamber (right panel). Samples filtered (0.2 μm).

3.1.3 Oxidation of V(IV) by Fe oxides

Due to the observation of increased dissolved Fe within the high treatment experiment, we explored the possibility of V(IV) mediated reductive dissolution of goethite using an additional control experiment exposing high concentration of V(IV) to goethite in the absence of birnessite. 90 mM V(IV) was incubated with 6.48 g of goethite in batch incubator and any aqueous Fe(II) generated was quantified using ferrozine assay. Results for the control experiment are shown in Figure 6; Fe(II) concentration reaches a maximum concentration of near 4 µM within the first hour and then appears to remain low throughout the rest of incubation demonstrating negligible Fe(II) remains in solution. Although Fe(II) concentrations were detectable (equivalent to 0.004% of V(IV) added), the level is extremely low given the concentration of V(IV) added. This may be due to minimal oxidation of V(IV) by Fe oxides or rapid oxidation of Fe(II) by V(V) that is generated.

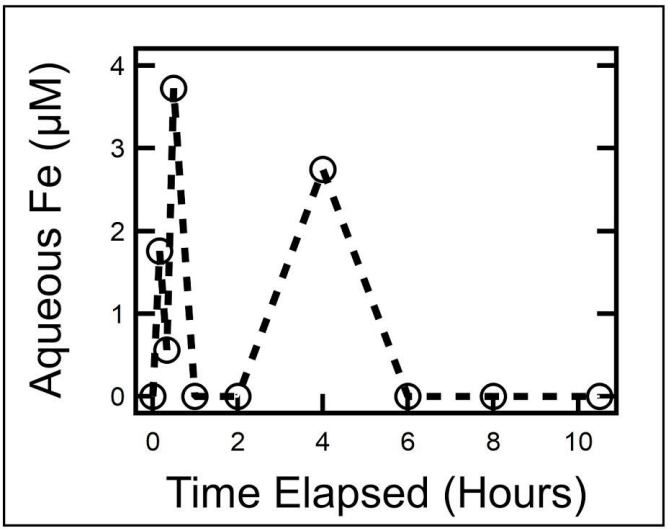

Fig. 6. Aqueous phase concentrations of Fe (II) µM (C) from incubation of 90mM V(IV) and goethite from 0 to 10.5 hours. Samples filtered and analyzed via ferrozine assay and spectrophotometer calibrated to 562 nm.

3.2 Solid phase acid digestion analysis

Slurry samples containing suspended solids were digested with strong acid and analyzed for total Mn, Fe, and V concentrations. V concentrations as determined by acid digestion are shown in Figure 7 for the low V concentration treatment experiment. Adsorption of V on birnessite remains constant at approximately 0.5 μmol g^{-1} or less throughout the experiment (Figure 7A), while V association with goethite is higher initially within the first 10 hours of reaction, reaching a maximum of 2.5 μmol g^{-1}, then decreasing to near detection limit by 96 hours (Figure 7B).

Reductive dissolution of birnessite during V(IV) oxidation leads to increased dissolved Mn in solution that can diffuse into the opposing goethite chamber. Therefore, Mn concentrations were also quantified in goethite solid phase digestions, which showed an initial peak in Mn associated with the Fe oxides, reaching a maximum mass per mass of 20 μmol g^{-1} at the beginning of the reaction (Figure 7D). Mn associated with goethite decreases over time with a similar trend to V dynamics, reaching near 0 mass per mass by 96 hours. This demonstrates both V and Mn are initially adsorbed followed by gradual desorption over the course of a few days. Some Fe was detected in the birnessite solid phase digestions, with a maximum of 5 μmol g^{-1} that is more or less maintained throughout the experiment except for a sharp decrease by 96 hours (Figure 7C).

Solid phase digestion results show different trends in sorption of V during the high V treatment experiments (Figure 8). Sorption of V increases over time on the birnessite solid (Figure 8A), whereas mass associated with goethite decreases over time (Figure 8B). Total mass of V associated with the birnessite were approximately 8 to 12 times higher in the high concentration treatment as compared to the low treatment experiment; V mass

associated with goethite during the high concentration treatment, however, was similar to the low treatment and exhibited a similar trend in desorption. Fe mass associated with birnessite were also minor and was generally lower than in the low treatment experiment (Figure 8C), whereas Mn associated with goethite exhibited an increasing trend over time (Figure 8D).

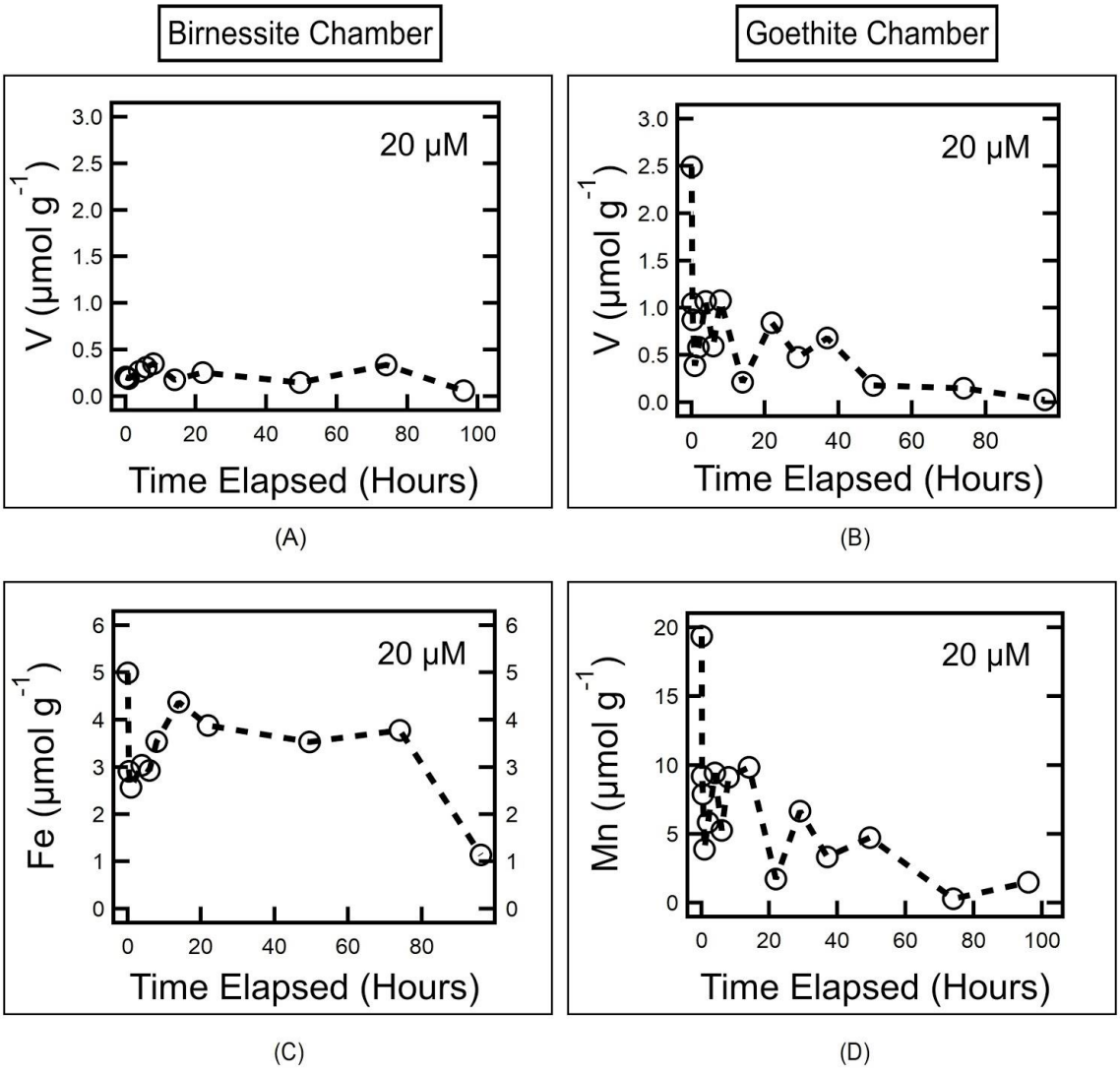

Fig. 7. Solid phase concentrations from 20 µM V(IV) experiment sampled from birnessite chamber (left panel) and goethite chamber (right panel) as determined by acid digestion and ICP-OES.

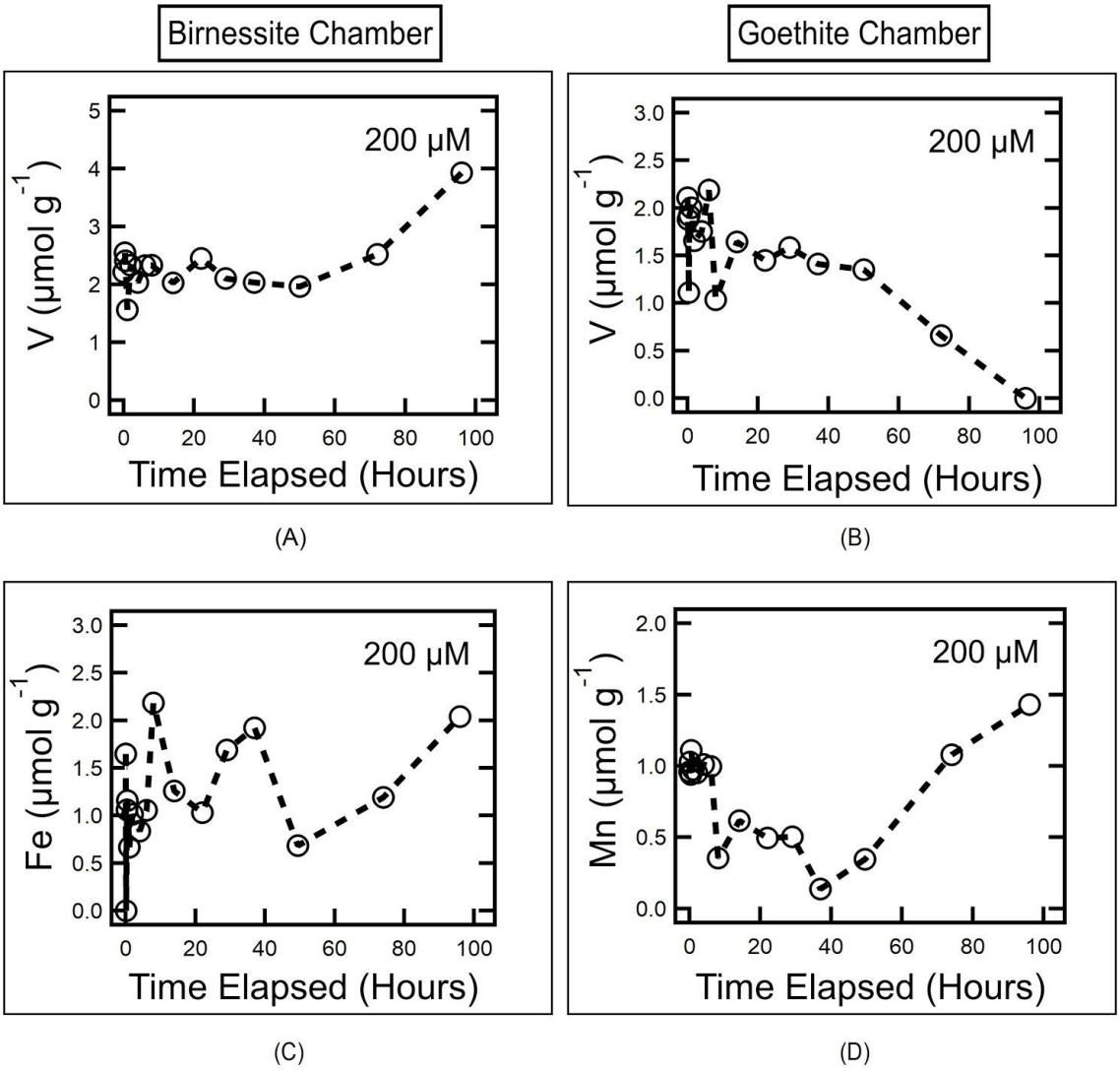

Fig. 8. Solid phase concentrations from 200 µM V(IV) experiment sampled from birnessite chamber (left panel) and goethite chamber (right panel) as determined by acid digestion and ICP-OES.

3.3 EXAFS and XANES analysis of adsorbed V

X-ray absorption spectroscopy provides *in situ* information on oxidation state and coordination chemistry of V associated with birnessite and goethite within the Donnan experiments. Solids were packed on ashless filters and exposed to X-ray beams above

and below the V K-edge using a soft X-ray line (BL 4-3) at Stanford Synchrotron Radiation Lightsource. Linear combination fitting (LCF) was used to determine the ratio of V(IV) to V(V) from XANES spectra taken of goethite and birnessite solids at the beginning and end of the experiments. Our results demonstrate that 73.2% of V adsorbed on birnessite was present as V(IV) after 30 seconds in the 90 mM control (Figure 9). By 96 hours, 51.5% of adsorbed V was V(V) demonstrating substantial but incomplete oxidation upon the birnessite surface by the end of the experimental period. This result is confirmed by the mixture of V(IV) and V(V) found in aqueous phase as indicated by the greenish-yellow color of the solution (Figure 2E).

In the low concentration 20 μM donnan experiment, V associated with birnessite and goethite at 30 seconds is 100% V(IV) (Figure 10C and D). After reaction for 96 hours, 52.8% of V associated with goethite was present as V(V) (Figure 10D). Only V(IV) was detected as adsorbed on birnessite during the initial timepoint (data not available for end point) (Figure 10C). V speciation in the high 200 μM concentration treatment Donnan experiment, ratio of V(IV):V(V) remained approximately 50:50 from 30 seconds to 96 hours in the birnessite chamber (Figure10A), while V associated with goethite was oxidized over the course of the experiment rising from 35.1% V(V) at the initial time point to 76.6% by 96 hours (Figure 10B).

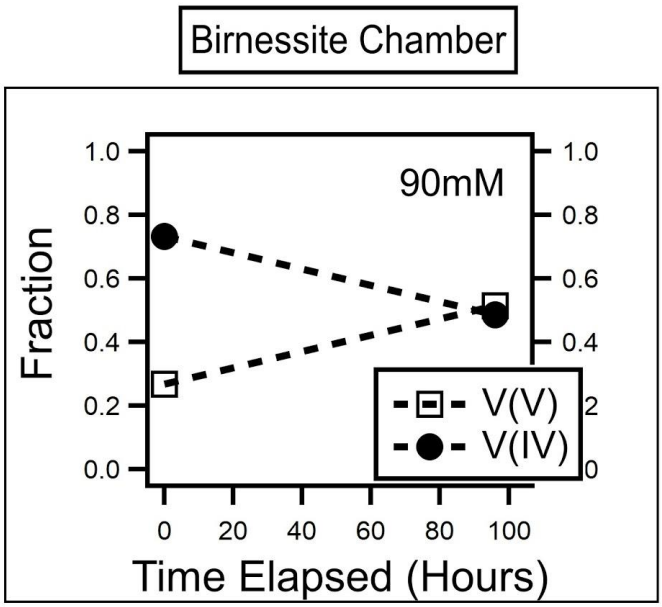

Fig. 9. Fractional distribution of V(IV)/V(V) in the 90mM V(IV) experiment based on linear cominational fitting from $VOSO_4$ V(IV) and Na_3VO_4 V(V) standards.

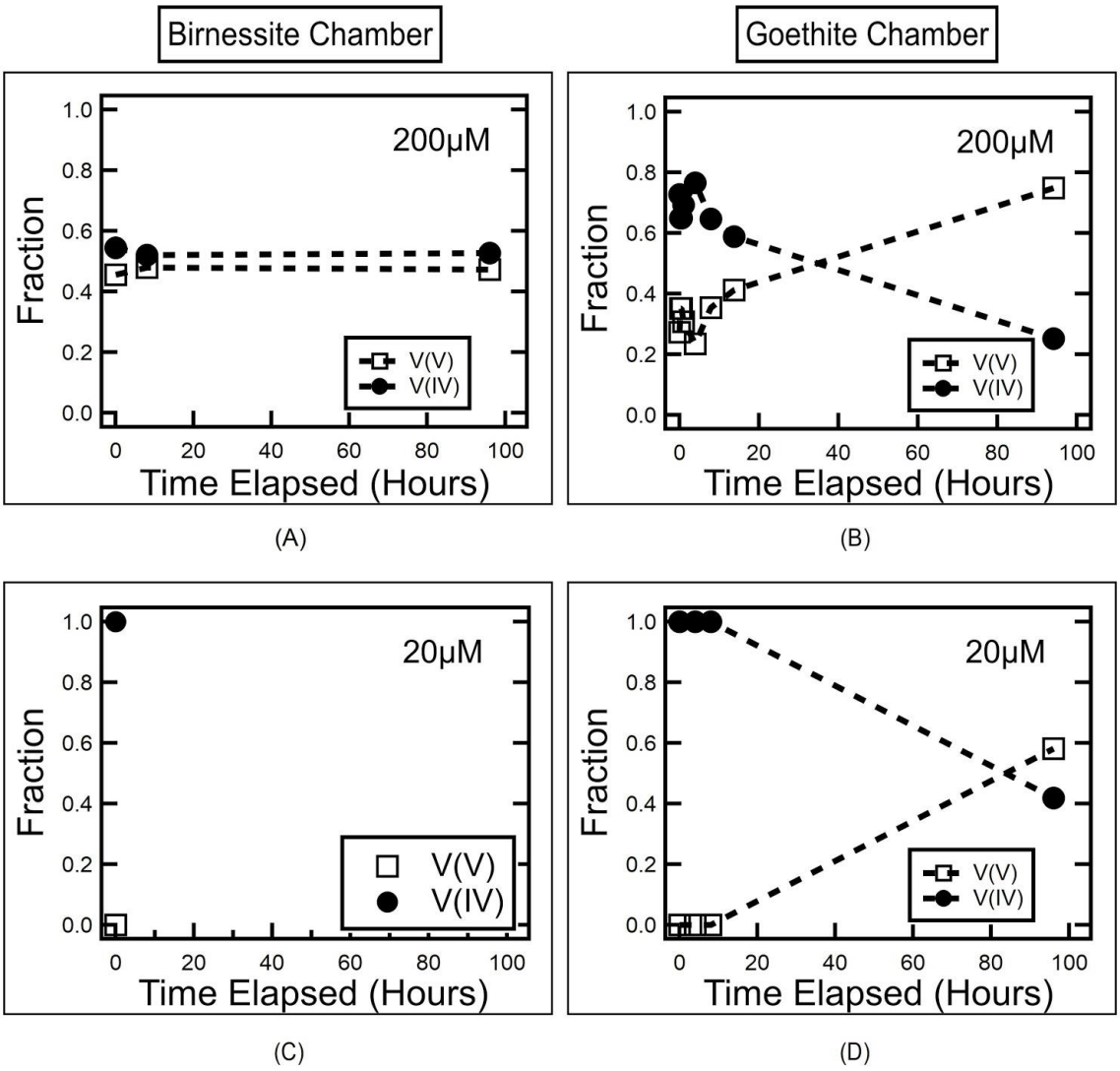

Fig. 10. Fractional distribution of V(IV)/V(V) based on linear cominational fitting from $VOSO_4$ V(IV) and Na_3VO_4 V(V) standards. 200 µM V(IV) concentration experimental samples are represented in (A) and (B) and 20 µM experimental samples are represented in (C) and (D) with birnessite chambers represented in the left panel and goethite chambers in the right panel.

3.4 Scanning electron microscopy and EDX analysis on solid phase

Birnessite synthesized from the method developed by McKenzie (1971) exhibited characteristic poorly crystalline granular and platy morphologies as shown by SEM imaging (Figure 11A). Goethite (provided by STREM chemicals) exhibited a cylindrical morphology ranging from 0.5 to 1 μm in length (Figure 11B). Solid phase digestion from the high concentration V treatment experiment showed the possibility of Fe being transported from the goethite chamber into the birnessite chamber, where Fe concentrations associated with the solids appeared to peak at 2 and 8 hours after V(IV) injection (Figure 8C). Solids taken before and after these time points were visualized using SEM and results are shown in Figure 11. SEM images of solid samples in the birnessite chamber at 30 minutes shows the possible presence of goethite particles less than 1 μm in length (Figure 11C). Samples taken from the goethite chamber at 30 minutes (Figure 11D), 6 hours (Figure 11F), and 96 hours (Figure 11H) do not contain any particles with morphological resemblance to birnessite nor show presence of Mn in EDX spectra. However, EDX spectra indicate the presence of Fe in platy birnessite structure at 96 hours, while the poorly crystalline granular structures revealed a smaller Fe peak (Figure 12).

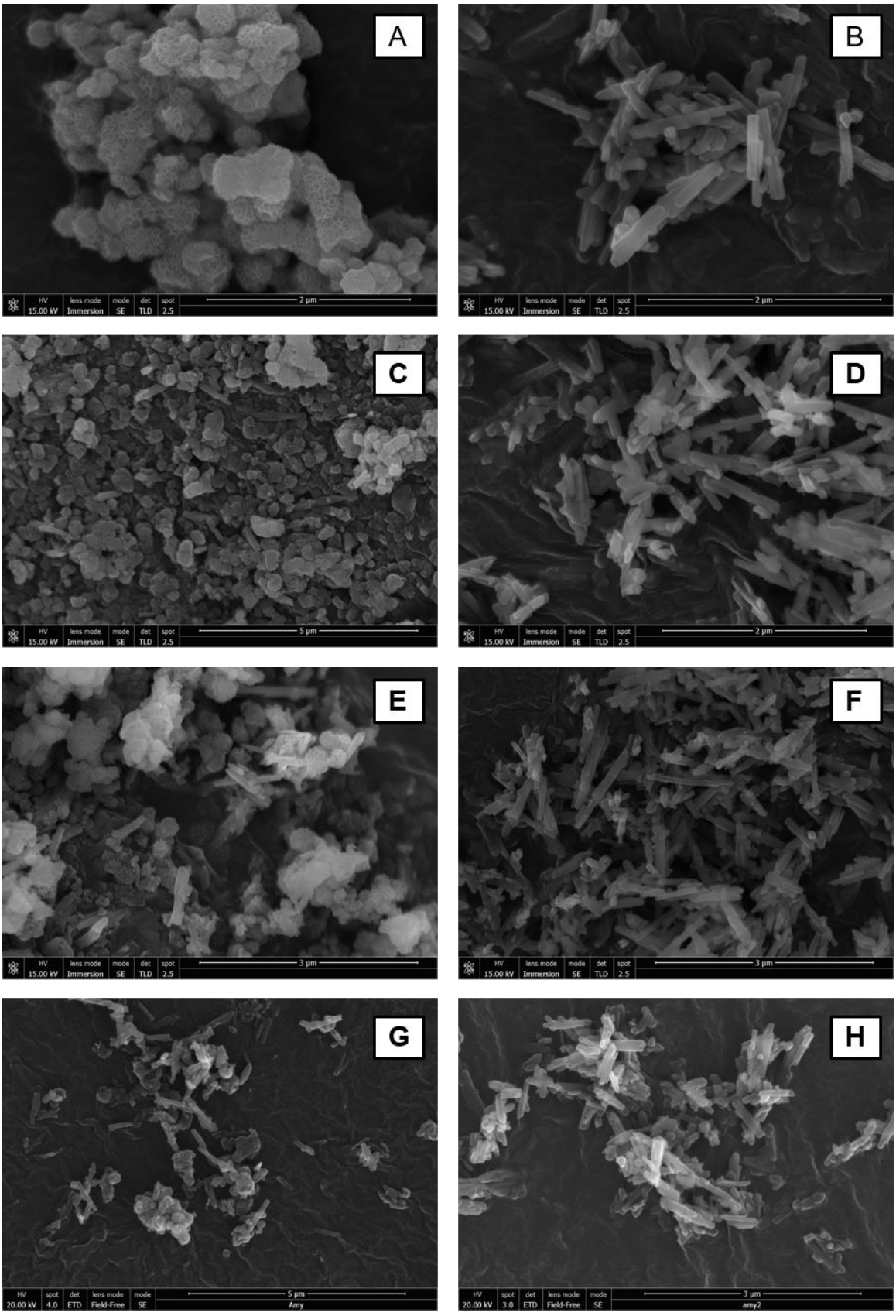
A
HV 15.00 kV | lens mode Immersion | mode SE | det TLD | spot 2.5 | 2 µm
B
HV 15.00 kV | lens mode Immersion | mode SE | det TLD | spot 2.5 | 2 µm
C
HV 15.00 kV | lens mode Immersion | mode SE | det TLD | spot 2.5 | 5 µm
D
HV 15.00 kV | lens mode Immersion | mode SE | det TLD | spot 2.5 | 2 µm
E
HV 15.00 kV | lens mode Immersion | mode SE | det TLD | spot 2.5 | 3 µm
F
HV 15.00 kV | lens mode Immersion | mode SE | det TLD | spot 2.5 | 3 µm
G
HV 20.00 kV | spot 4.0 | det ETD | lens mode Field-Free | mode SE | 5 µm | Amy
H
HV 20.00 kV | spot 3.0 | det ETD | lens mode Field-Free | mode SE | 3 µm | amy2

Fig.11. SEM images of birnessite oxide (A), goethite oxide (B), and solid phase samples of 200 µM V(IV) experiment (C) - (F) washed in acetone. Samples from 200 µM V(IV) experiment include birnessite chamber at 30 minutes (C), goethite chamber at 30 minutes (D), birnessite chamber at 6 hours (E), goethite chamber at 6 hours (F), birnessite chamber at 96 hours (G), and goethite chamber at 96 hours (H).

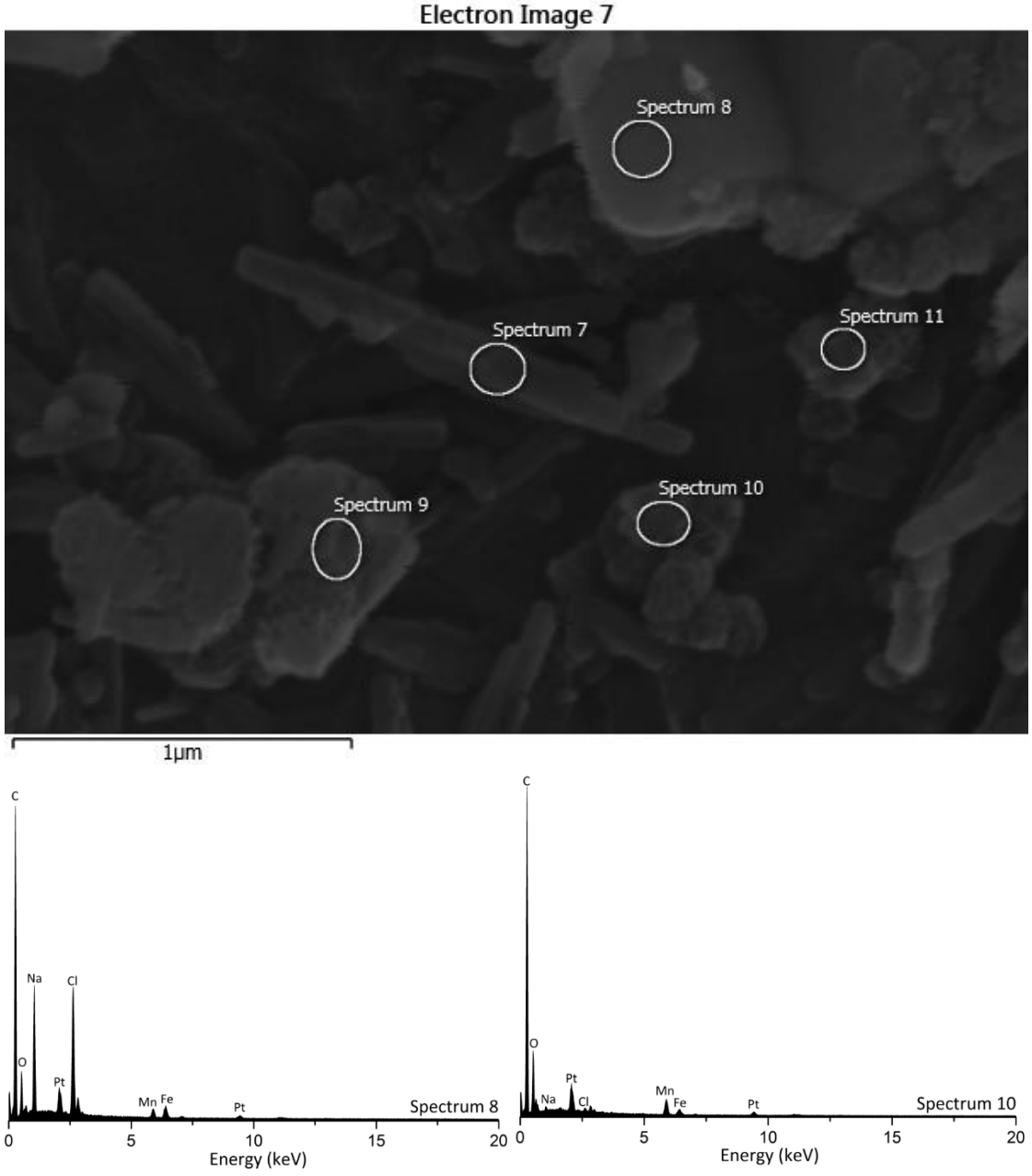

Fig.12. SEM-EDX image of solid state sample of birnessite chamber of 200 µM V(IV) experiment at 96 hours. Goethite and birnessite crystal structures present represented by three different morphologies. Platy birnessite structure (spectrum 8 and 9), poorly crystalline amorphous granule (spectrum 10 and 11), and cylindrical goethite structure (spectrum 7). Elemental intensities of spectrum 8 and 10 represented in graphs below.

3.5 X-ray diffraction analysis of solid phase

Solid phase samples were taken at 96 hours from both chambers of high concentration treatment experiment and from goethite chamber only of low concentration treatment for XRD analysis (Figure 13). Diffractograms show very little to no change in goethite morphology over the course of the experiments at both V concentrations. Analysis of birnessite samples from the high concentration treatment show presence of goethite peaks.

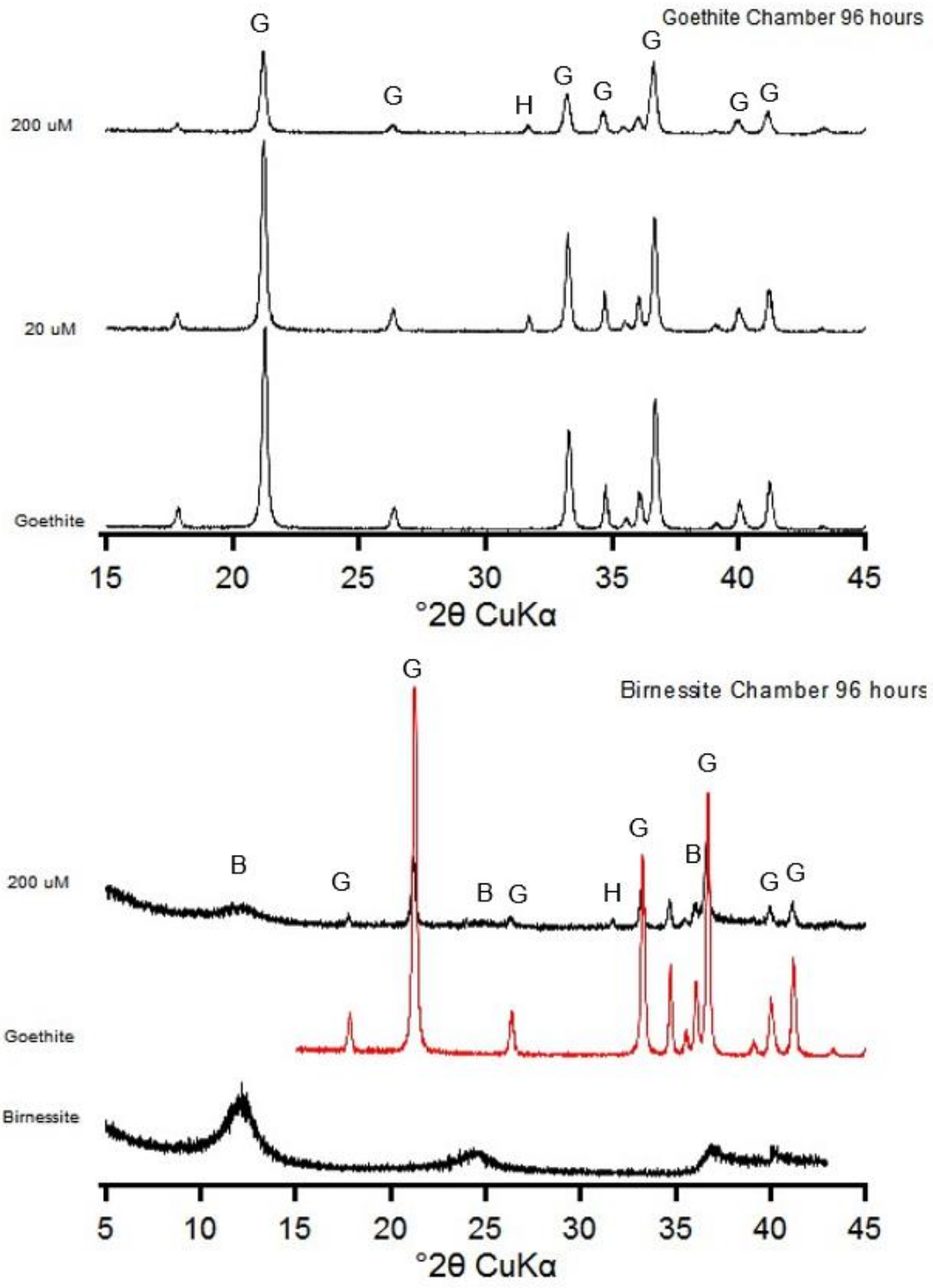

Figure 13. XRD patterns of oven dried slurry from goethite and birnessite chambers at 96 hours. Goethite and birnessite used as references. Defining peaks labelled with "G" for definitive goethite peaks, "B" for definitive birnessite peaks, and "H" for definitive halite peaks.

4. Discussion

Utilizing the Donnan reactor, we were able to examine the interactions between V(IV) and representatives of common soil Fe and Mn oxides simultaneously within a diffusion-limited environment. Our results demonstrate definitively that birnessite, a poorly crystalline Mn(III/IV) oxide is able to oxidize V(IV) to V(V) with subsequent adsorption on both birnessite and goethite surfaces.

A proposed reaction mechanism based upon the interaction of V(IV) with permanganate studied by Moore and Hicks (1975) is provided here of the rate-limiting versus rapid steps involving birnessite mediated oxidation of V(IV) via a predicted two-step mechanism with the reaction of the Mn(III/IV)-VO^{2+} complex likely occurring rapidly.

1. $Mn(III/IV) + VO^{2+} \rightarrow [Mn(III/IV)\text{-}VO^{2+}]$ *rate-limiting*

2. $[Mn(III/IV)\text{-}VO^{2+}] \rightarrow Mn(III) + VO_2^{+}$ *rapid*

3. $Mn(III) + VO^{2+} \rightarrow Mn(II) + VO_2^{+}$ *rate-limiting*

Batch incubation of goethite with excess V(IV) appeared to demonstrate that limited reductive dissolution of goethite occurs with <<1% of Fe(II) being measured in solution during multiple time periods through the incubation. However, appreciable concentrations of dissolved Fe was detected in the high concentration treatment Donnan experiment within the goethite chamber after V(IV) injection. These confounding results demonstrate that additional control experiments need to be performed to definitively understand the redox cycling of Fe(III) oxides in the presence of various concentrations of V(IV). Some possible interactions between Fe(III) and V(IV) within the Donnan experiments are

provided here. Thermodynamically, it is favorable for V(IV) to reduce Fe(III) (Rosseinsky, 1972), however, these calculations have not been performed for Fe(III) within an oxide matrix. In the case that goethite is reductively dissolved by V(IV) within the Donnan, Fe(II) generate could then possibly be 1) re-adsorbed on goethite, 2) reoxidized by V(V) generated during the reaction, or 3) reoxidized by birnessite when transported into the opposing chamber. If only low concentrations of Fe(II) are release, it is possible that the methods used in this project would not be able to detect any of these three pathways accurately. However, if goethite reduction by V(IV) is in fact appreciable, it would have been expected that high concentrations of Fe(II) would be released when V(IV) was added in excess to goethite in batch experiments (Figure 6). It is also possible that any V(V) generated through Fe(III) oxidation of V(IV) would then rapidly reoxidize Fe(II), making Fe(II) difficult to detect. Better understanding of the kinetics of these reactions would also help to tease apart the reaction network.

The lack of V in the EDX spectra during SEM analysis may be due to a combination of method specific steps and desorption mechanisms influenced by V oxidation reactions. Samples were washed with acetone prior to SEM imaging, which possibly contributed to the low V detected in EDX spectra as compared to what is expected from solid phase digestions. Mn oxides can adsorb V(IV) on surface sites, however, adsorbed V can then desorb rapidly after oxidation to V(V) (Moore and Hicks, 1975). Low concentrations of V in aqueous solution and higher concentrations in acid digestion data indicate a possible combination of precipitation of V as polynuclear species or complexed with reduced Mn and Fe species.

The presence of polynuclear species of V may be an explanation for the major differences in aqueous and solid phase dynamics seen between the high and low concentration treatment experiments. The higher concentration is well above the 100 µM threshold at which V polymers are expected to form at circumneutral pH (Larson, 1995). Formation of polymers is rapid upon oxidation of V(IV) where tetravanadates and decavanadates are dominant at pH ranges of 6-8 forming up to 50-60 molar percent of aqueous V input (Larson, 1995). V polymers can form into aggregates greater than 5 µm (Wu, 2017) and can have improved sorption capacities of metal cations than any other V forms (Guzman et al., 2002; SenGupta, 2007). Therefore, Mn(II) produced from the oxidation of V(IV) by birnessite has the potential to adsorb onto polynuclear vanadium species formed during the high concentration treatment experiment. Comparison of the 90 mM and 200 µM V(IV) experiments demonstrates that release of dissolved Mn from birnessite upon reaction with V(IV) is concentration dependent and likely related to polynuclear species formation. In the presence of 200 µM V(IV), Mn(II) release was inhibited whereas in the presence of 90 mM V(IV) a high concentration of dissolved Mn(II) was released into the aqueous phase. A possible cause to an inhibition of Mn(II) release in the 200 µM experiment is that V(IV) was added directly into the chamber containing birnessite, whereas in the 90 mM control, V(IV) was injected into the opposing chamber and V(IV) came into contact with birnessite in low concentrations controlled by diffusion-limited transport through the filter membrane. The immediate contact of the 200 µM V(IV) with birnessite may have caused polymeric V(V) to coat the Mn oxide surface, which then inhibits release of Mn(II) into the aqueous phase as a form of surface passivation. This would also explain the lack of surface sorption observed over the course of the experiment, possibly due to blockage of surface sites by polymeric V(V) species. Use of near-edge X-ray absorption spectroscopy (NEXAFS), XPS

or other surface analyses and NMR on birnessite particles exposed to low (<200 µM) and high (~200 µM) V(IV) concentrations may reveal the speciation of V associated with the birnessite surfaces.

Birnessite shows two distinct morphologies of platy and poorly-crystalline solids. From the SEM-EDX spectra, the platy morphologies show a greater intensity of Fe than the poorly-crystalline morphologies indicating each morphology has different sorptive capacities. Isomorphic substitution of Fe or V into the birnessite platy morphology is not likely due to the platy structure being present in pure birnessite form and XRD patterns showing birnessite and goethite oxides at 96 hours and lack of any other mineral forming.

5. Conclusion

Vanadium oxidation and retention in natural anoxic environments rich in iron and manganese oxides is highly dependent on V concentration, diffusion rate of aqueous species, and availability and stability of oxides. Our results indicate that V interacts with birnessite with a concomitant release of dissolved Mn(II) and V(V) into solution. V interaction with goethite exhibits rapid sorption of V onto the oxides and a possible oxidation reaction of V(IV) by Fe(III) resulting in the release of V(V) and Fe(II) within the first 6 hours upon exposure to both high (200 µM) and low (20 µM) concentrations of V(IV). The mechanisms responsible for the appearance of Fe in aqueous samples within Donnan experiments upon introduction of V(IV) are not well understood and requires additional studies. As the reaction progressed within the Donnan reactor, goethite shows a decrease in V retention after the initial oxidation reactions within the first 6 hours. Birnessite adsorbed higher mass of V than goethite in competitive systems where both oxides were

present and may therefore play a significant role in V immobilization within redox fluctuating environments where Mn oxides can accumulate (Gillispie et al., 2016).

Retention and sorption is highly dependent on concentration of V where concentrations above 100 µM or concentrations of polynuclear species formation, form polymers of V(V) that can average 5 µm in size and retain aqueous Mn and V. Additional research is needed to confirm formation of polynuclear vanadate and the sorptive capacity of aqueous Mn and Fe ions of these polymers.

In general, V may be immobilized from transport through adsorption on oxides when V concentrations are low or through precipitation/condensation reactions when V concentrations are high. Mn oxides have greater retention capacities of V than Fe oxides although V as V(IV) and V(V) are weakly held. The results of this study indicate that the overall interaction of V with competing Mn and Fe oxides in anoxic groundwater systems may have significant impacts on V redox cycling and mobilization of V into groundwater.

References

Briand, Laura, Horacio Thomas, and Edgardo Donati. 1996. “Vanadium(V) Reduction in Thiobacillus Thiooxidans Cultures on Elemental Sulfur.” *Biotechnology Letters* 18 (5): 505–8. doi:10.1007/BF00140192.

Dixon, Joe B., and G. Norman White. 2002. “Manganese Oxides.” *Soil Mineralogy with Environmental Applications* sssabookseries (soilmineralogyw): 367–88. doi:10.2136/sssabookser7.c11.

Geneva, World Health Organization. 1988. “Vanadium.” http://www.inchem.org/documents/ehc/ehc/ehc81.htm.

Gillispie, Elizabeth C., Robert E. Austin, Nelson A. Rivera, Rick Bolich, Owen W. Duckworth, Phil Bradley, Aziz Amoozegar, Dean Hesterberg, and Matthew L. Polizzotto. 2016. “Soil Weathering as an Engine for Manganese Contamination of Well Water.” *Environmental Science & Technology* 50 (18): 9963–71. doi:10.1021/acs.est.6b01686.

Guzmán, J., I. Saucedo, R. Navarro, J. Revilla, and E. Guibal. 2002. “Vanadium Interactions with Chitosan: Influence of Polymer Protonation and Metal Speciation.” *Langmuir* 18 (5): 1567–73. doi:10.1021/la010802n.

Hem, John D. 1977. “Reactions of Metal Ions at Surfaces of Hydrous Iron Oxide.” *Geochimica et Cosmochimica Acta* 41 (4): 527–38. doi:10.1016/0016-7037(77)90290-3.

Hope, Bruce K. 2008. “A Dynamic Model for the Global Cycling of Anthropogenic Vanadium.” *Global Biogeochemical Cycles* 22 (4). doi:10.1029/2008GB003283.

James Olopade, and James R Connor. 2011. “Vanadium and Neurotoxicity: A Review.” https://www.researchgate.net/publication/285738434_Vanadium_and_neurotoxicity_A_review.

Larson, John W. 1995. “Thermochemistry of Vanadium(5+) in Aqueous Solutions.” *Journal of Chemical & Engineering Data* 40 (6): 1276–80. doi:10.1021/je00022a030.

Mckenzie, R. M. 1971. “The Synthesis of Birnessite, Cryptomelane, and Some Other Oxides and Hydroxides of Manganese: Mineral.” *Mag*, 493–502.

Moore, Fred M., and Kenneth W. Hicks. 1975. “Mechanism of the Permanganate Ion Oxidation of vanadium(IV).” *Inorganic Chemistry* 14 (2): 413–16. doi:10.1021/ic50144a041.

Myers, Judith M., William E. Antholine, and Charles R. Myers. 2004. “Vanadium(V) Reduction by Shewanella Oneidensis MR-1 Requires Menaquinone and Cytochromes from the Cytoplasmic and Outer Membranes.” *Applied and*

Environmental Microbiology 70 (3): 1405–12. doi:10.1128/AEM.70.3.1405-1412.2004.

Peacock, Caroline L., and David M. Sherman. 2004. “Vanadium(V) Adsorption onto Goethite (α-FeOOH) at pH 1.5 to 12: A Surface Complexation Model Based on Ab Initio Molecular Geometries and EXAFS Spectroscopy.” *Geochimica et Cosmochimica Acta* 68 (8): 1723–33. doi:10.1016/j.gca.2003.10.018.

Ravel, B., and M. Newville. 2005. “ATHENA, ARTEMIS, HEPHAESTUS: Data Analysis for X-Ray Absorption Spectroscopy Using IFEFFIT.” *Journal of Synchrotron Radiation* 12 (Pt 4): 537–41. doi:10.1107/S0909049505012719.

Rosseinsky, D. R. 1972. “Aqueous Electron-Transfer Reactions. Vanadium(IV) as Reductant Compared with Iron (II).” *Chemical Reviews* 72 (3): 215–29. doi:10.1021/cr60277a002.

SenGupta. 2007. “Ion Exchange and Solvent Extraction: A Series of Advances, Volume 18.” *CRC Press*. July 4. https://www.crcpress.com/Ion-Exchange-and-Solvent-Extraction-A-Series-of-Advances-Volume-18/SenGupta/p/book/9780849373978.

Sexstone, A. J., N. P. Revsbech, T. B. Parkin, and J. M. Tiedie. 1985. “Direct Measurement of Oxygen Profiles an Denitrification Rates in Soil Aggregates.” *Journal - Soil Science Society of America (USA)*. http://agris.fao.org/agris-search/search.do?recordID=US8619330.

Tokunaga, T. K., J. Wan, M. K. Firestone, T. C. Hazen, E. Schwartz, S. R. Sutton, and M. Newville. 2001. “Chromium Diffusion and Reduction in Soil Aggregates.” *Environmental Science & Technology* 35 (15): 3169–74.

USGS. 2015. “California GAMA Program: Ground-Water Quality Data in the Northern San Joaquin Basin Study Unit, 2005 - ds_196.pdf.” Accessed October 25. http://pubs.usgs.gov/ds/2006/196/ds_196.pdf.

Wehrli, Bernhard, and Werner Stumm. 1988. “Oxygenation of vanadyl(IV). Effect of Coordinated Surface Hydroxyl Groups and Hydroxide Ion.” *Langmuir* 4 (3): 753–58. doi:10.1021/la00081a045.

Wehrli, Bernhard, and Werner Stumm. 1989. “Vanadyl in Natural Waters: Adsorption and Hydrolysis Promote Oxygenation.” *Geochimica et Cosmochimica Acta* 53 (1): 69–77. doi:10.1016/0016-7037(89)90273-1.

Wright, Michael T., and Kenneth Belitz. 2010. “Factors Controlling the Regional Distribution of Vanadium in Ground Water.” *Ground Water* 48 (4): 515525.

Wright, Michael T., Kenneth G. Stollenwerk, and Kenneth Belitz. 2014. “Assessing the Solubility Controls on Vanadium in Groundwater, Northeastern San Joaquin Valley, CA.” *Applied Geochemistry* 48 (September): 41–52. doi:10.1016/j.apgeochem.2014.06.025.

Ying, Samantha C., Benjamin D. Kocar, and Scott Fendorf. 2012. “Oxidation and Competitive Retention of Arsenic between Iron- and Manganese Oxides.” *Geochimica et Cosmochimica Acta* 96 (November): 294–303. doi:10.1016/j.gca.2012.07.013.

Ying, Samantha C., Benjamin D. Kocar, Sarah D. Griffis, and Scott Fendorf. 2011. “Competitive Microbially and Mn Oxide Mediated Redox Processes Controlling Arsenic Speciation and Partitioning.” *Environmental Science & Technology* 45 (13): 5572–79. doi:10.1021/es200351m.

Supplemental Information

ICP-OES calibration points

	Analyte			
Calibration point	V	Fe	Mn	Na
1	3.926 μM	3.581 μM	3.6405 μM	0.435 mM
2	0.1963 mM	0.179 mM	0.182 mM	2.175 mM
3	0.3926 mM	0.3581 mM	0.364 mM	4.349 mM
4	1.5704 mM	1.7906 mM	1.8202 mM	
5	9.815 mM	8.9534 mM	9.1011 mM	

ICP-OES analysis detection limits

Analyte	Detection Limit
V	0.118 μM
Mn	0.0269 μM
Fe	0.4314 μM
Na	10.44 μM

Diffusion coefficient calculations

Brilliant blue dye is injected into one side of a constructed donnan reactor with 0.2 μm polycarbonate filter filled with DDI water. Concentrations of blue dye is measured on both

injection chamber and chamber in which dye is diffusing into via spectrophotometer calibrated to 610 nm.

The diffusion coefficient (DAB) used in was calculated using following equation:

$$\gamma = -\frac{2SD_{AB}H}{LV}$$

Where ɣ (mol L^{-1} s^{-1}) is the slope of the line for a plot of y versus time, S (m^2) is the surface area of the semipermeable membrane between the two cells, DAB (m^2 s^{-1}) is the diffusion coefficient for the solute, H (m^3 g^{-1}) is the partition coefficient (assuming H=1 in homogeneous conditions), L(m) is the length of the reactor, and V (m^3) is the volume of each reactor cell.

$$y = ln\frac{(conc_1 - conc_2)}{100}$$

The slope of the line, ɣ, is calculated from the above equation where $conc_1$ is the concentration of blue dye in the chamber where blue dye is injected. $Conc_2$ is the concentration of blue dye in the chamber in which the dye is diffusing into.

N2-BET conditions

Degassing conditions for BET isotherms included an evacuation phase of 2℃ min^{-1}, a target temperature of 70℃, an evacuation rate of 2 mmHg sec^{-1}, a heating phase of 2℃ min^{-1}, a holding temperature of 90℃, and a holding time of 700 min.